

Dynamics of magnetic microbubble transport in blood vessels

Jie Chen(陈杰), Chenghui Wang(王成会), and Runyang Mo(莫润阳)
Citation: Chin. Phys. B, 2023, 32 (**9**): 094302. DOI: 10.1088/1674-1056/aca14b
Journal homepage: http://cpb.iphy.ac.cn; http://iopscience.iop.org/cpb

What follows is a list of articles you may be interested in

Effect of magnetic field on expansion of ferrofluid-encapsulated microbubble

Zhiwei Du(杜芷玮), Fan Li(李凡), Ruiqi Pan(潘瑞琪), Runyang Mo(莫润阳), and Chenghui Wang(王成会)
Chin. Phys. B, 2023, 32 (**6**): 064302. DOI: 10.1088/1674-1056/acc1d2

Wideband frequency-dependent dielectric properties of rat tissues exposed to low-intensity focused ultrasound in the microwave frequency range

Xue Wang(王雪), Shi-Xie Jiang, Lin Huang(黄林), Zi-Hui Chi(迟子惠), Dan Wu(吴丹), and Hua-Bei Jiang
Chin. Phys. B, 2023, 32 (**3**): 034305. DOI: 10.1088/1674-1056/ac7453

Quantitative ultrasound brain imaging with multiscale deconvolutional waveform inversion

Yu-Bing Li(李玉冰), Jian Wang(王建), Chang Su(苏畅), Wei-Jun Lin(林伟军), Xiu-Ming Wang(王秀明), and Yi Luo(骆毅)
Chin. Phys. B, 2023, 32 (**1**): 014303. DOI: 10.1088/1674-1056/ac6dad

Nonlinear oscillation characteristics of magnetic microbubbles under acoustic and magnetic fields

Lixia Zhao(赵丽霞), Huimin Shi(史慧敏), Isaac Bello, Jing Hu(胡静), Chenghui Wang(王成会), and Runyang Mo(莫润阳)
Chin. Phys. B, 2022, 31 (**3**): 034302. DOI: 10.1088/1674-1056/ac1f01

Dynamics of an ultrasound contrast agent microbubble near spherical boundary in ultrasound field

Ji-Wen Hu(胡继文), Lian-Mei Wang(王练妹), Sheng-You Qian(钱盛友), Wen-Yi Liu(刘文一), Ya-Tao Liu(刘亚涛), Wei-Rui Lei(雷卫瑞)
Chin. Phys. B, 2019, 28 (**11**): 114301. DOI: 10.1088/1674-1056/ab4d3f

---

Dynamics of magnetic microbubble transport in blood vessels

Jie Chen(陈杰), Chenghui Wang(王成会)[†], and Runyang Mo(莫润阳)[‡]

Institute of Shaanxi Key Laboratory of Ultrasonics, Shaanxi Normal University, Xi'an 710119, *China*

(Received 8 September 2022; revised manuscript received 7 November 2022; accepted manuscript online 9 November 2022)

Magnetic microbubbles (MMBs) can be controlled and directed to the target site by a suitable external magnetic field, and thus have potential in therapeutic drug-delivery application. However, few studies focus on their dynamics in blood vessels under the action of magnetic and ultrasonic fields, giving little insight into the mechanism generated in diagnostic and therapeutic applications. In this study, equations of MMBs were established for simulating translation, radial pulsation and the coupled effect of both. Meanwhile, the acoustic streaming and shear stress on the vessel wall were also presented, which are associated with drug release. The results suggest that the magnetic pressure increases the bubble pulsation amplitude, and the translation coupled with pulsation is manipulated by the magnetic force, causing retention in the target area. As the bubbles approach the vessel wall, the acoustic streaming and shear stress increase with magnetic field enhancement. The responses of bubbles to a uniform and a gradient magnetic field were explored in this work. The mathematical models derived in this work could provide theoretical support for experimental phenomena in the literature and also agree with the reported models.

Keywords: magnetic microbubbles, targeted drug delivery, ultrasound, magnetic field

PACS: 43.35.+d, 43.25.+y, 47.55.dp **DOI:** 10.1088/1674-1056/aca14b

1. Introduction

Ultrasound combined with microbubble contrast agents has been widely demonstrated as a method of improving the delivery of drugs and genes *in vitro* and *in vivo*. However, the technique is limited by the relatively low delivery efficiencies achieved. Encapsulated microbubbles coupled with magnetic nanoparticles are referred to as magnetic microbubbles (MMBs), and are regarded as a recent development with the potential to greatly improve the efficacy of drug delivery and procedure sonoporation.[1–4] The shell elasticity allows volume oscillations in an acoustic field, which can be more easily controlled by an external magnetic field and demonstrate great potential as a drug delivery vehicle and multi-modal imaging tool.[5–7]

Gene transfection enhanced by MMBs was first demonstrated by Stride *et al.*,[8] and then confirmed by Mulvana *et al.*[9] and Vlaskou *et al.*[10] One possible mechanism is that both the concentration and proximity of the MMBs to the target cells are improved by the magnetic field.[11] However, this assumption needs to be further confirmed[12–14] and more experiments are needed. The effects of nanoparticles on the dynamic and acoustic responses of MMBs have been characterized.[15,16] The harmonic response and cavitation activity have been investigated experimentally.[17,18] Zhao *et al.*[19] found experimentally that the magnetic susceptibility is proportional to the square of MMB radii. Meanwhile, MMBs also show powerful potential in tumor therapy and targeted drug delivery.[20,21] Both magnetic nanoparticles and nanodrugs can be released from oscillating MMBs.[12,14] Zhang *et al.*[2] reported an application in sonothrombolysis and confirmed that MMBs can be retained by a rotational magnetic field against blood flow. Recently, a series of sonodynamic therapies induced by oscillating MMBs in external fields were further verified.[22,23] Several specific devices were designed to maximize the superiority for tumor treatments.[13,24,25]

The kinetics and regulation of MMBs are the basis of its application. To describe the volume oscillations exposed to ultrasound, Mulvana *et al.*[16] conducted a preliminary modelling study. A fixed volume fraction of solid nanoparticles was used to examine the influence of an additional magnetic layer. Recently, Zhao *et al.*[26] developed a multilayer magnetic shell model and the nonlinear oscillating characteristics were numerically evaluated. However, these studies have their limitations, because they ignore the influence of an applied magnetic field and non-spherical pulsation. Previous numerical studies on bubble dynamics in a magnetic field often were replaced by the dynamic of one or more non-magnetic bubbles in magnetic fluids. In this way, Lind[27] simulated the dynamics of non-spherical MMBs and showed that the magnetic susceptibility difference between bubbles and the ambient fluid can provide an additional means of flow control. Malvar *et al.*[28] formulated a new version of the Rayleigh–Plesset equation by considering the magnetic stress contribution and proved that the bubble oscillating motion can be controlled and its collapse avoided when a high magnetic field is applied. Chen *et al.*[29] expanded this work and found that the vibration amplitude could be enhanced by the magnetic field. Unfortunately, the coupling effect between vibration and translation

[†]Corresponding author. E-mail: wangld001@snnu.edu.cn
[‡]Corresponding author. E-mail: mmrryycn@snnu.edu.cn

© 2023 Chinese Physical Society and IOP Publishing Ltd

has not been investigated and this incomplete understanding of the transport mechanism of MMBs makes some phenomena observed from experiments difficult to explain.

Mathematical study acts an important role in exploring this mechanism by offering detailed mechanical processes that would be difficult or impossible to see *in vitro* or *in vivo*. In this work, theoretical models are established to simulate the dynamics of MMB transport in blood vessels under acoustic pressure and magnetic fields. In addition, some parameters associated with drug release are also simulated, especially the shear stress generated by bubble pulsation, which increases with the intensity of the applied magnetic field. The study attempts to provide insight into the details of MMB motion during targeted transport and support some experimental conclusions.

2. Theory and method

2.1. Translation in blood vessels

MMBs transported in blood vessels are capable of targeted delivery and drug release when driven by ultrasound and magnetic fields. As shown in Fig. 1, typical processes were summarized as translation, pulsation and drug release. MMBs can be retained in the tumor region under the guidance of a magnetic field, and perform drug release behavior in ultrasound.

In a steady vessel flow, a single MMB is governed by three forces, expressed as

$$m_{\text{eff}}\frac{\mathrm{d}\boldsymbol{v}}{\mathrm{d}t} = \boldsymbol{F}_M + \boldsymbol{F}_{\text{buoy}} + \boldsymbol{F}_{\text{D}}, \tag{1}$$

where m_{eff} is the effective mass of the MMB including the added mass, and the three terms on the right side of Eq. (1) are the magnetic force, buoyancy and drag force, respectively.

In addition, m_{eff} is small enough relative to other factors, which means the terminal velocity can be rapidly obtained. The process of MMB transport in the target region is shown in Fig. 2. When MMBs arrive at the targeted region, $\boldsymbol{F}_{\text{M}}$ is generated by a linear Halbach array of magnets, which is used in the experiment work of Barnsley *et al.*[24] and expressed by

$$\boldsymbol{F}_{\text{M}} = \boldsymbol{m}\cdot\nabla\boldsymbol{B} = \frac{\chi_{\text{b}}}{\mu_0}B\frac{\mathrm{d}B}{\mathrm{d}z}\hat{\boldsymbol{e}}_z, \tag{2}$$

where $\boldsymbol{m}$ is the total magnetic moment of the magnetic nanoparticles, χ_{b} is the magnetic susceptibility of the bubbles, μ_0 is the permeability of vacuum space, and B is the magnetic induction. The expressions $\chi_{\text{b}} = (6\times10^{-6}\ \text{m})R^2$, $\mathrm{d}B/\mathrm{d}z = 900\,\mathrm{e}^{(-0.75z_{\text{mag}}/\text{mm})}T/m$ and $B = 1.1\,\mathrm{e}^{(-0.63z_{\text{mag}}/\text{mm})}T$ are cited from the literature.[19,24]

The vessel is assumed to be a laminar cylindrical channel in the x-axis direction,[24] and the liquid flow rate v_{F} is given by

$$\boldsymbol{v}_{\text{F}} = 2v_{\text{A}}\left(1-\left(\frac{y}{R_{\text{C}}}\right)^2-\left(\frac{z}{R_{\text{C}}}\right)^2\right)\hat{\boldsymbol{e}}_x, \tag{3}$$

where v_{A} is the mean velocity and R_{C} is the channel radius.

Taking blood as a Newtonian fluid, the drag force $\boldsymbol{F}_{\text{D}}$ is followed by Stokes' law and given by viscous drag

$$\boldsymbol{F}_{\text{D}} = 6\pi\eta_{\text{L}}R(\boldsymbol{v}_{\text{F}}-\boldsymbol{v}), \tag{4}$$

where η_{L} is the liquid viscosity, R is the temporary radius and $\boldsymbol{v}$ is the velocity vector of the transport MMBs. Only the two dominant forces $\boldsymbol{F}_{\text{M}}$ and $\boldsymbol{F}_{\text{D}}$ are considered in this model; one can obtain the result by combining Eqs. (1)–(4), given as

$$\boldsymbol{v} = \boldsymbol{v}_{\text{F}} + \frac{\boldsymbol{F}_{\text{M}}}{6\pi\eta_{\text{L}}R} = v_{\text{F}}\hat{\boldsymbol{e}}_x + v_z\hat{\boldsymbol{e}}_z. \tag{5}$$

If $\boldsymbol{F}_{\text{M}}$ is uniformly distributed in the local region, the component of $\boldsymbol{v}$ in z-direction v_z is approximated as a constant. This method has been verified by simulations and experiments in the literature.[24]

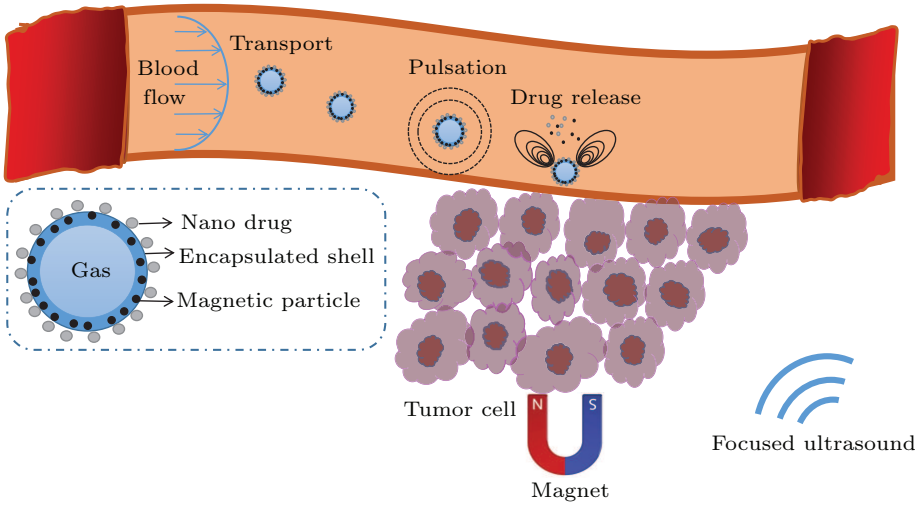


Fig. 1. Sketch of MMBs used for targeted drug delivery.

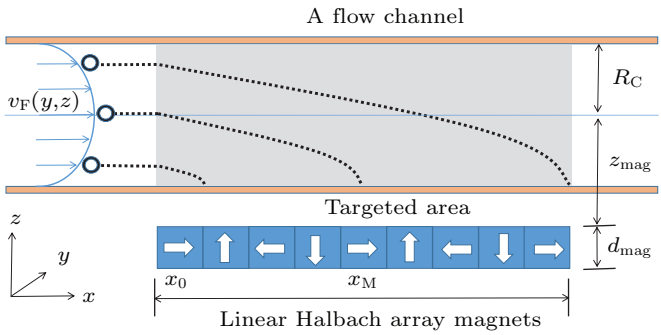


Fig. 2. Targeted delivery of MMBs in a flowing channel. The channel radius is R_C with a flow in the x-direction, and each bubble is trapped in the target area marked by the shaded region from x_0 to x_M. Linear Halbach array magnets with thickness d_{mag} are fixed at a distance z_{mag} from the channel center. The dotted lines show the bubble trajectories under the attraction of the magnets.

Primarily, our model is based on the one-dimensional cylindrical channel flow along the x-direction according to Eq. (3), and the magnetic force is applied in the z-direction. There is no driving force in the y-direction, so the displacement in the y-direction is ignored. Further, the coordinate components $x(t)$ and $z(t)$ are obtained by integrating the velocity components in Eq. (5). Taking the original coordinate position as $(x_0,\ y_0,\ z_0)$, $x(t)$ and $z(t)$ can be represented as follows:[24]

$$\begin{aligned} z(t) &= z_0 + v_z t, \\ x(t) &= x_0 + 2v_A t\left(1 - \frac{1}{R_C^2}\left(\frac{1}{3}(v_z t)^2 + z_0 v_z t + y_0^2 + z_0^2\right)\right). \end{aligned} \tag{6}$$

Due to the strong magnetic force, MMBs are assumed to have no slippery contact with the channel wall. Thereby, the capture efficiency is expressed as[24,25]

$$\text{capture efficiency} = 0.601\left(\frac{v_z}{v_A}\frac{x_M}{R_C}\right)^{0.522} \times 100\%. \tag{7}$$

2.2. Dynamic model of coupled motion

Previous studies have shown that magnetic nanoparticles have little effect on acoustic response, and MMBs are also not obviously affected by magnetic fields.[16] Donikove's model[30] describes the vibration of a thin-shell bubble in an infinite liquid, represented as

$$\begin{aligned} &R\ddot{R} + \frac{3}{2}\dot{R}^2 \\ &= \frac{1}{\rho_L}\left[P_{g0}\left(\frac{R_0}{R}\right)^{3\gamma} - \frac{2\sigma}{R} - 4\eta_L\frac{\dot{R}}{R} - P_0 - P_{ac}(t) - S\right], \end{aligned} \tag{8}$$

where R and R_0 are the transient radius and the initial radius, respectively. $\dot{R}$ is the bubble wall velocity, the liquid density and viscosity are ρ_L and η_L, respectively, σ is the surface tension, P_{g0} is the equilibrium pressure, γ is the polytrophic exponent, $P_{ac}(t) = P_a \sin(2\pi f t)$ is the acoustic driving pressure, and S represents the role of the encapsulated shell and is described by

$$S = 4\kappa\left(\dot{R}/R\right)\frac{\dot{R}}{R^2} + 4\zeta\frac{R_0}{R}\left(\frac{1}{R_0} - \frac{1}{R}\right), \tag{9}$$

where $\kappa\left(\dot{R}/R\right) = \kappa_0 + \kappa_1\dot{R}/R$ is the shell surface viscosity (in $\text{kg}\cdot\text{s}^{-1}$) and ζ is the shell surface elasticity (in $\text{N}\cdot\text{m}^{-1}$). The values of shell parameters κ_0, κ_1 and ζ are obtained from the literature,[30] and some observations[17,21,30] show that the stiffness and viscosity of the shell are related to magnetic particle concentration. When MMBs move in the vessel,[31,32] the kinetic energy of the system is contributed by pulsation and translation, which is defined as

$$T = 2\pi\rho_L R^3\dot{R}^2(1+\alpha+\beta) + 2\pi\rho_L R^3\frac{\dot{x}^2+\dot{z}^2}{6}, \tag{10}$$

where $\alpha = \frac{2RL_C}{R_C^2}\left(1 - \frac{3}{2}\frac{R_C}{L_C}\right)$, $\beta = \frac{\varepsilon^2}{1+\varepsilon}\frac{R}{l_d}$ are determined by the vessel boundary, R_C is the channel radius and L_C the length, ε is the curvature of the channel, and l_d is the distance between the bubble center and vessel wall.

Considering the work done by pulsation and external forces $\boldsymbol{F}_{ex}$ acting on MMBs, the potential energy[33] of the system is

$$U = -\frac{4\pi}{3}R^3\Delta P - (x\hat{e}_x + z\hat{e}_z)\cdot\boldsymbol{F}_{ex}. \tag{11}$$

From the right terms of Eq. (8), ΔP includes an additional magnetic pressure P_M, and P_M is given by Lind:[27,34]

$$\begin{aligned} \Delta P &= P_{g0}\left(\frac{R_0}{R}\right)^{3\gamma} - \frac{2\sigma}{R} - 4\eta_L\frac{\dot{R}}{R} \\ &\quad - P_0 - P_{ac}(t) + P_M - S, \end{aligned} \tag{12}$$

$$P_M = \frac{\Delta\chi}{2\mu_0}B_0^2, \tag{13}$$

where μ_0 is the vacuum permeability, and B_0 is the magnetic field strength and generally taken as 1–2 T.[8,16,27] The magnetic susceptibility difference $\Delta\chi$ is a dimensionless value between the MMBs and the ambient fluid. $\boldsymbol{F}_{ex}$ in Eq. (11) denotes the external forces acting on the MMBs, and can be written as

$$\begin{aligned} \boldsymbol{F}_{ex} &= -12\pi\eta_L R\left((\dot{x} - v_F)\hat{e}_x + \dot{z}\hat{e}_z\right) \\ &\quad + F_M\hat{e}_z + \frac{\rho_L}{4\pi(2l_d)^2}\dot{V}_b^2\hat{e}_z. \end{aligned} \tag{14}$$

The right terms of Eq. (14) correspond to Levich viscous drag,[35] magnetic force and secondary Bjerknes force,[36] and the bubble volume is V_b.

In addition, the Lagrangian quantity of the system is

$$\begin{aligned} L &= 2\pi\rho_L R^3\left(\dot{R}^2(1+\alpha+\beta) + \frac{\dot{x}^2+\dot{z}^2}{6}\right) \\ &\quad + \frac{4\pi}{3}R^3\Delta P + (x\hat{e}_x + z\hat{e}_z)\cdot\boldsymbol{F}_{ex}. \end{aligned} \tag{15}$$

If other dissipative factors are ignored, the Lagrange equation is expressed as

$$\frac{\mathrm{d}}{\mathrm{d}t}\frac{\partial L}{\partial \dot{q}}-\frac{\partial L}{\partial q}=0, \tag{16}$$

taking R, x, z and $\dot{R}$, $\dot{x}$, $\dot{z}$ as generalized coordinates and velocities, respectively. This operation yields the equations of MMB dynamics

$$R\ddot{R}(1+\alpha+\beta)+\frac{3}{2}\dot{R}^2\left(1+\frac{4}{3}\alpha+\frac{4}{3}\beta\right) = \frac{\Delta P}{\rho_{\mathrm{L}}}+\frac{\dot{x}^2+\dot{z}^2}{4}, \tag{17}$$

$$\ddot{x}+\frac{3\dot{R}\dot{x}}{R}=\frac{3F_x}{2\pi\rho_{\mathrm{L}}R^3}, \tag{18}$$

$$\ddot{z}+\frac{3\dot{R}\dot{z}}{R}=\frac{3F_z}{2\pi\rho_{\mathrm{L}}R^3}. \tag{19}$$

Equations (17)–(19) are the coupled formulas describing the radial pulsation and translation of MMBs in the vessel. The contributions of the magnetic field and vessel wall are considered, such as the magnetic pressure, magnetic force, Bjerknes force, velocity gradient and the system kinetic energy adjusted by the vessel wall, which are the main factors in describing the boundary effect of fluid–solid interaction. This model has a similar form to the non-magnetic bubbles in a magnetic fluid,[28,29] and it also agrees with the reported models of gas bubbles in a channel and near a curved wall.[31,32] For more complex cases, the reflection and absorption of the vessel wall, even for non-spherical jets, remain to be further clarified.

Assuming MMBs vibrating at small amplitudes, the eigenfrequency[37] is obtained by Eq. (17) as

$$f_0^*=f_0\frac{1}{\sqrt{1+\frac{2R_0L_{\mathrm{C}}}{R_{\mathrm{C}}^2}\left(1-\frac{3}{2}\frac{R_{\mathrm{C}}}{L_{\mathrm{C}}}\right)+\frac{\varepsilon^2}{1+\varepsilon}\frac{R_0}{l_{\mathrm{d}}}}}, \tag{20}$$

$$f_0=\frac{1}{2\pi R_0\sqrt{\rho}}\sqrt{3\gamma P_0+\frac{2(3\gamma-1)\sigma}{R_0}+\frac{4\zeta}{R_0}}, \tag{21}$$

where f_0^* and f_0 correspond to the vessel and infinite environment, respectively.

2.3. Drug release dynamics

Safely increasing transfection efficiencies in sonoporation (the amount of drug uptake by cells) remains an important issue and the shear stress caused by microstreaming has been demonstrated as an effective means. When a drug particle is detached from a MMB, the force balance relationship[12] is satisfied:

$$\frac{\mathrm{d}u_{\mathrm{P}}}{\mathrm{d}t}=\frac{\rho_{\mathrm{L}}}{\rho_{\mathrm{L}}C_{\mathrm{A}}+\rho_{\mathrm{P}}}\frac{\mathrm{d}u_{\mathrm{L}}}{\mathrm{d}t}-\frac{18\eta_{\mathrm{L}}}{d_{\mathrm{P}}^2(\rho_{\mathrm{L}}C_{\mathrm{A}}+\rho_{\mathrm{P}})}(u_{\mathrm{P}}-u_{\mathrm{L}}), \tag{22}$$

where d_{P} is the particle diameter, u_{P} is the particle velocity, $u_{\mathrm{L}}=\frac{R^2}{r^2}\frac{\mathrm{d}R}{\mathrm{d}t}$ is the liquid velocity induced by bubble vibration, and C_{A} is the viscous drag coefficient.

The microstreaming, generated by vibrating bubbles when they approach the wall, can be described by $\psi(r,\theta)$ in spherical coordinates.[38] The dimensionless velocity u^* is a function of θ and given by Eq. (24).

$$\psi(r,\theta)=\frac{AR_0^4\omega}{r}\cos^2\theta\sin^2\theta, \tag{23}$$

$$u^*=\frac{|u/A|}{R_0\omega}\left(\frac{r}{R_0}\right)^3=\sqrt{\frac{\sin^2(4\theta)}{4\sin^2\theta}+\sin^2\theta\cos^4\theta}, \tag{24}$$

where A is the dimensionless source strength depending on the oscillation mode of the bubble. To simplify the description, a dimensionless radial function $f(r)=AR_0^3\omega/r$ is introduced to demonstrate the streamline distribution.

According to Nyborg's theory,[39,40] if the pulsating bubble is close to the vessel wall, the x component of shear stress on the cells can be quantified by

$$\tau_{xz}=2(\rho_{\mathrm{L}}\eta_{\mathrm{L}})^{1/2}(\pi f)^{3/2}\frac{\xi_{\mathrm{m}}^2}{R_0}\left(\frac{R_0}{l_{\mathrm{d}}}\right)^5\frac{2\delta(1-2\delta^2)}{(1+\delta^2)^4}, \tag{25}$$

where ξ_{m} is the pulsating amplitude and $\delta=x/l_{\mathrm{d}}$.

3. Numerical simulation

The parameters used in numerical analysis are as follows: $R_0=2$ μm, $P_0=10^5$ Pa, $\rho_{\mathrm{L}}=10^3$ kg·m^{-3}, $\sigma=0.085$ N·m^{-1}, $\eta_{\mathrm{L}}=10^{-3}$ Pa·s, $P_{\mathrm{a}}=60$ kPa, $\Delta\chi=0.1$, and $f=1$ MHz. Typical parameters of the shells of MMBs are $\kappa_0=1.45\times10^{-8}$ kg·s^{-1}, $\kappa_1=6\times10^{-15}$ kg and $\zeta=0.2$ N·m^{-1}. Moreover, the drug particles are simulated with $d_{\mathrm{P}}=100$ nm, $\rho_{\mathrm{P}}=3\times10^3$ kg·m^{-3} and $C_{\mathrm{A}}=0.5$.

3.1. Transport in gradient magnetic field

3.1.1. Magnetic field analysis

The strength and gradient of the magnetic field are essential for MMB localization. Figure 3(a) plots the fitting curve of B as a function of z_{mag} given as $B=1.1\,\mathrm{e}^{(-0.63z_{\mathrm{mag}}/\mathrm{mm})}$ T. It matches the experimental data[24] (blue dots in Fig. 3(a)) very well. The gradient of the magnetic field depends on z_{mag} and is expected to be $\mathrm{d}B/\mathrm{d}z=900\,\mathrm{e}^{(-0.75z_{\mathrm{mag}}/\mathrm{mm})}$ T/m (inset plot in Fig. 3(a)). The values of $B\cdot\mathrm{d}B/\mathrm{d}z$ are 18 T^2·m^{-1} and 53.2 T^2·m^{-1} in the literature,[8,11] which agree with our data of 18.1 T^2·m^{-1} and 54.6 T^2·m^{-1} at $z_{\mathrm{mag}}=2.9$ mm and 2.1 mm, respectively. The magnetic force F_{M} acting on MMBs is related to z_{mag} in Fig. 3(b). A semilog plot is presented to emphasize the exponential properties of F_{M} with z_{mag}. The marked data of 100 μm radius at $z_{\mathrm{mag}}=4$ mm is 2.142×10^{-7} N, which agrees with experimental observations.[19] The F_{M} marked as 8.568×10^{-11} N for a radius of 2 μm is about 2500 times for 100 μm. This variation

follows the rule $F_M \sim R^2$ due to magnetic nanoparticle numbers. When MMBs are attracted by magnets, their position and acting forces are changed with time. Larger bubbles carry more magnetic particles and produce stronger magnetic force. In Fig. 3(c), a bubble with 2 μm radius moves from $z = 3$ mm to $z = 0$ mm at the latest and takes 0.09 s, which is much longer than a larger one. This suggests that the size sorting of MMBs could be assisted by an external force,[41] and a better operation on aggregation would be realized by the attached magnetic force. Figure 3(d) shows the competition between forces on a bubble with 2 μm radius at $z_0 = 3$ mm. When the bubble is close to the magnets, the velocity is gradually accelerated by the magnetic force, and the drag force is also increased until terminal equilibrium is reached. As expected, the values of both the added mass force and buoyancy force are smaller than magnetic and drag forces; this observation supports the simplification of Eq. (5).

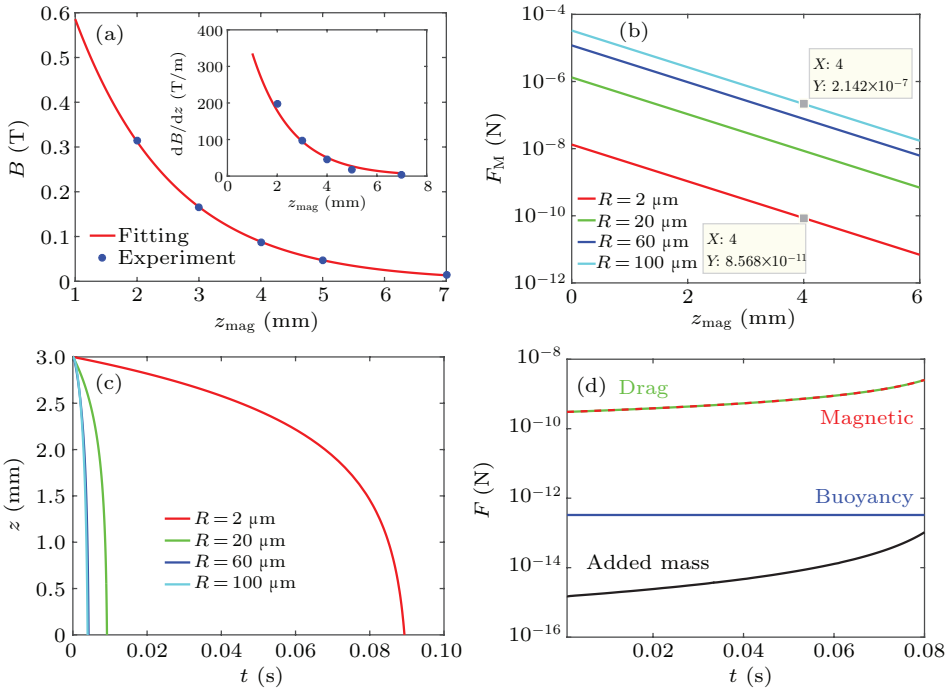


Fig. 3. Responses of MMBs to the linear Halbach array magnets. (a) Character of gradient magnetic field; (b) relationship of $F_M \sim z_{mag}$; (c) transport in z-direction guided by magnets; (d) forces acting on a bubble of $R = 2$ μm at $z_0 = 3$ mm.

3.1.2. Transport trajectory

In a vessel of $R_C = 0.25$ mm, MMBs moving from $x_0 = 0$ mm to $x_M = 2$ mm along the x axial direction are manipulated by the linear Halbach array magnets. For mean flow velocities of $v_A = 20$ mm·s^{-1} and 40 mm·s^{-1}, trajectories are shown in Figs. 4(a) and 4(b), respectively, and each horizontal line corresponds to a starting position. As an example for comparison, the black line is retained at $x = 2$ mm for 40 mm·s^{-1} and $x = 1$ mm for $v_A = 20$ mm·s^{-1}. Higher velocity v_A produces a horizontal displacement with a longer distance. Smaller distance to the magnets leads to better capture of MMBs with a shorter horizontal displacement, while higher flow velocity weakens the capture efficiency. The red line in Fig. 4(c) is the fitting curve from Eq. (7) that matches the calculated results (statistics from a large number of tracks), indicating that capture efficiency decreases as v_A increases, and the capture behavior observed in experiments can also be quantified by Eq. (7).[24,25] In other words, Eq. (7) can serve as a simple method to predict the capture efficiency without calculating tracks. The distance to the magnets is also an essential parameter in MMB capture. The relationship between translation velocity v_z and separation distance z_{mag} is shown in Fig. 4(d), Eq. (5) shows an exponential relationship between them, and the marked data represent the speed at several specific distances. Above all, the trajectories of MMBs can be established by the model shown in Eq. (6), and the capture efficiency between calculation and the analytical formula has been well verified.

3.1.3. Capture efficiency

MMBs can be localized at the target region when they are attracted by a gradient magnetic field. Capture efficiency is studied by Eq. (5) using the control variable method. These parameters include the component of transport velocity in the z direction v_z, mean velocity v_A, vessel radius R_C and magnet length x_M; the results are shown in Figs. 5(a)–5(d). When $R_C = 0.25$ mm, the efficiency increases with improved v_z and x_M (Figs. 5(a) and 5(b)) and decreases with v_A (Fig. 5(c)), so a higher moving velocity and longer magnets can be more efficient, whereas a stronger flow velocity has the opposite effect. However, if v_A and x_M are constant, smaller R_C and larger v_z are more effective as shown in Fig. 5(d).

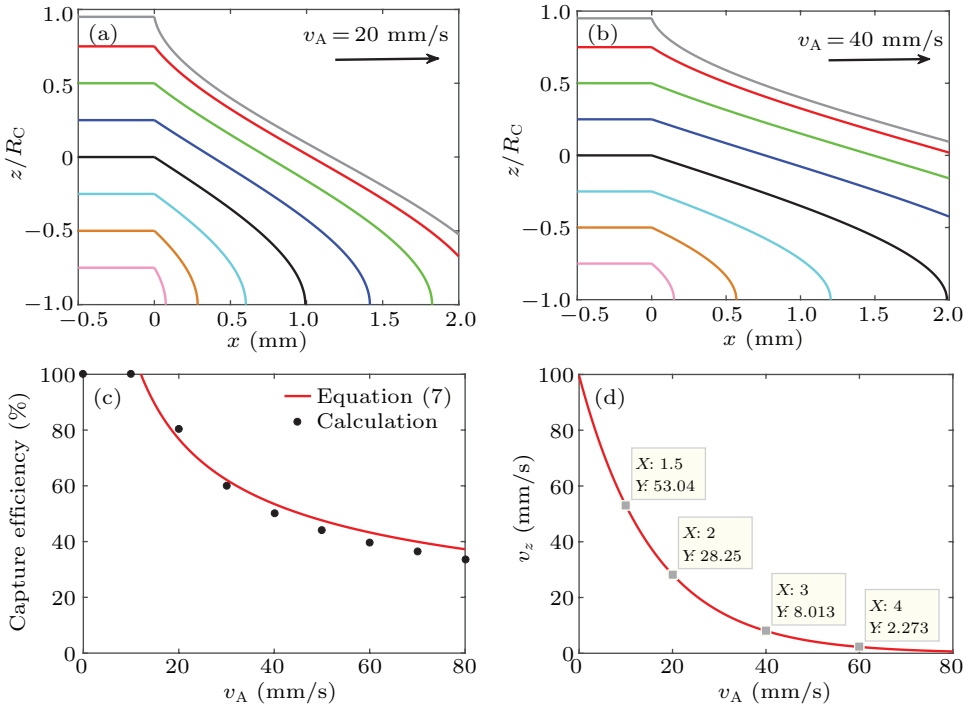


Fig. 4. Transport properties of MMBs in a blood vessel. (a) and (b) The trajectories in the x–z plane at $z_{mag} = 3.25$ mm, $v_A = 10$ mm·s^{-1} and 20 mm·s^{-1}, respectively; (c) capture efficiency related to v_A; (d) v_z determined by z_{mag}.

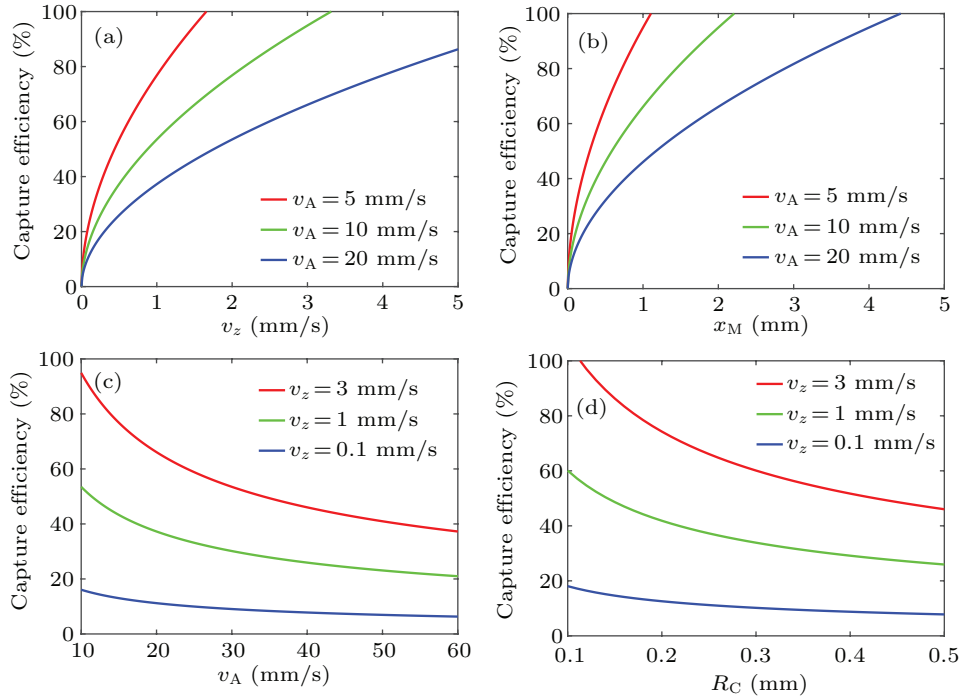


Fig. 5. Capture efficiency of MMBs. (a) $R_C = 0.25$ mm, $x_M = 2$ mm; (b) $v_z = 3$ mm·s^{-1}, $R_C = 0.25$ mm; (c) $x_M = 2$ mm, $R_C = 0.25$ mm; (d) $v_A = 20$ mm·s^{-1}, $x_M = 2$ mm.

3.2. Pulsation in uniform magnetic field

3.2.1. Pulsation in unbound case

To study MMBs pulsating in a uniform magnetic field, first, the unbound case without the vessel wall constraint was simulated. The R–t curves with code testing are shown in Fig. 6(a); the parameters used here are $R_0 = 1.4$ μm, $f = 3$ MHz and $P_a = 100$ kPa. The prediction of the proposed model (green line) matches well with the data (red circles) in the literature.[30] To highlight the effect of the shell, an unshelled bubble was used for comparison data (blue line). The shell effect reduces the amplitude and increases the harmonics.[42] Figure 6(b) shows the vibration of MMBs ($R = 2$ μm, $P_a = 60$ kPa and $f = 1$ MHz) in magnetic fields of $B_0 = 1$ T, 1.5 T and 2 T. The vibration amplitude increases with B_0 and one possible mechanism is that magnetic field pro-

motes acoustic response. Similar results were found in Lind's theoretical analysis of non-spherical bubbles in a magnetic liquid,[27] and it is also supported by violent bubble oscillation manipulated by external fields in a magnetic fluid[28,29] and electric medium.[43] Moreover, after removing the ultrasonic field at 6.5 μs, damping oscillations of MMBs are also displayed, and the final static radius is increased with the intensity of magnetic field.

As shown in Fig. 6(c), the oscillation amplitude near the resonance frequency increases significantly with magnetic field intensity. Considering $B_0 = 0$ T, the maximum amplitude corresponding to the frequency is 2.6 MHz, which agrees with the 2.63 MHz calculated by Eq. (24) using $\zeta = 0.2$ N·m^{-1}. Meanwhile, the resonant peak shifts from 2.6 MHz to 1.4 MHz after applying $B_0 = 2$ T, and the resonance frequency drops because the magnetic field increases the final static radius. Figure 6(d) depicts the curve of magnetic pressure P_M for $\Delta\chi = 0.01$, 0.05 and 0.1; the larger the susceptibility difference is, the faster P_M increases with B_0 improvement. Conversely, bubbles in liquid oxygen with susceptibility 0.0035 have a smaller magnetic pressure of 1.4 kPa at $B_0 = 1$ T,[34] which directly supports the idea that magnetic pressure is determined by the magnetic field and susceptibility difference between MMBs and the ambient fluid.

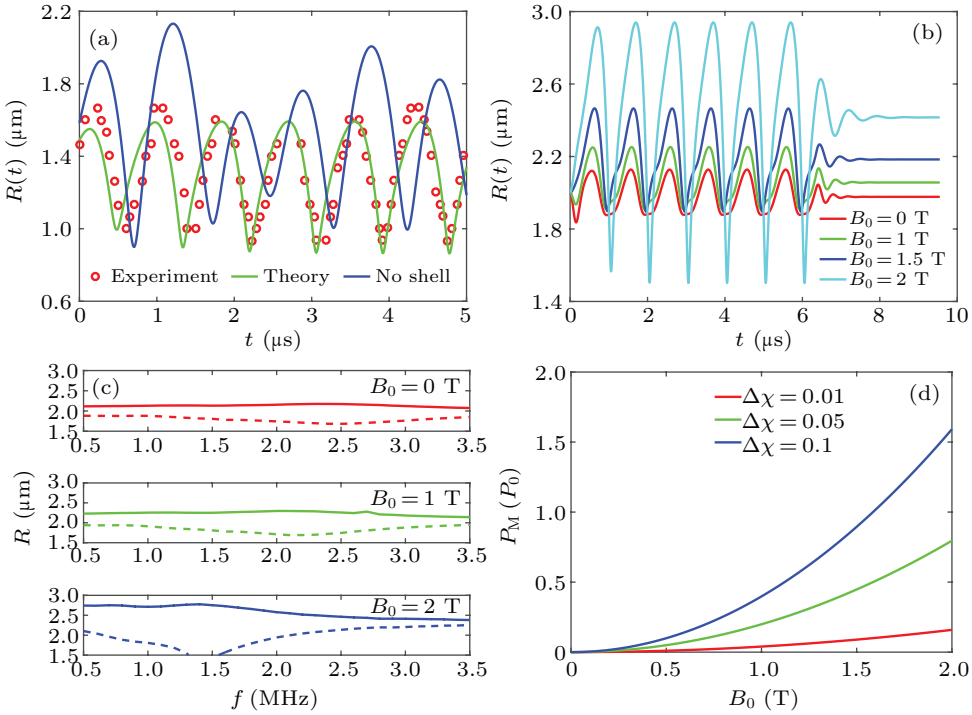


Fig. 6. MMBs vibrating in a uniform magnetic field. (a) Code testing and MMB analysis in $B_0 = 0$ T ($f = 3$ MHz, $P_a = 100$ kPa); (b) R–t curves adjusted by the magnetic field ($f = 1$ MHz, $P_a = 60$ kPa); (c) oscillating amplitude in $B_0 = 0$ T, 1 T and 2 T ($P_a = 60$ kPa), R_{max} (solid line) and R_{min} (dashed line); (d) P_M determined by B_0 and $\Delta\chi$.

3.2.2. Resonance frequency

First, the shell effect on resonance frequency f_0 is shown as an unbound case in Fig. 7(a). The hybrid shell has higher surface elasticity compared with an uncoated bubble and yields a higher f_0. The prediction of the green line with $\zeta = 0.3$ N·m^{-1} aligns with the experimental data,[44] and the discrepancy decreases with increasing bubble size. Moreover, f_0 can also be used to evaluate the shell elasticity.[45] As shown in Figs. 7(b) and 7(c), a larger R_C and further distance l_d yield a lower resonance frequency. Moreover, f_0^*/f_0 decreases greatly with increasing R and the observed rule is consistent with the literature,[46,47] indicating the reliability of this model.

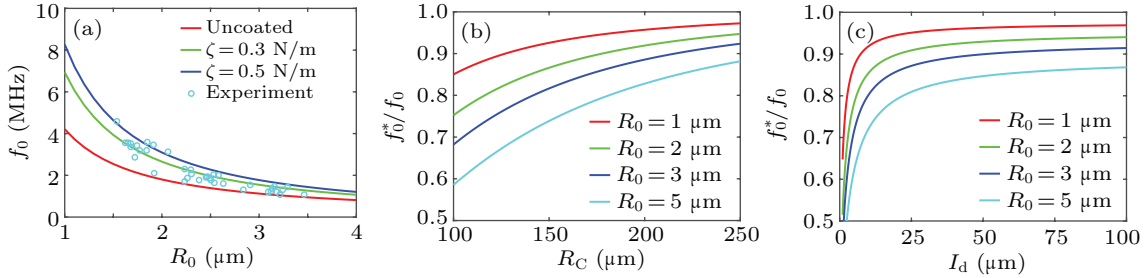


Fig. 7. Resonance frequency of single MMBs. (a) Unbound; (b) in the vessel center; (c) close to the vessel wall.

3.2.3. Pulsation near vessel wall

Oscillating MMBs near the wall were used to verify the validity of the model. The red circles in Fig. 8(a) represent the data carried by Garbin[48] and the green line is the predicted result of this model. The two results almost coincide and the deviation may be attributed to uncertain l_d or non-spherical pulsation. In contrast, a bubble far away from the wall is seen as a free one, shown as a blue line; a shorter period and larger amplitude imply that boundary constraints suppress oscillations.[49,50] As shown in Fig. 8(b), the boundary constraint causes a resonance frequency decrease, and the magnetic field obviously alters the oscillatory response when compared with the unconstrained case as shown in Fig. 6(c).

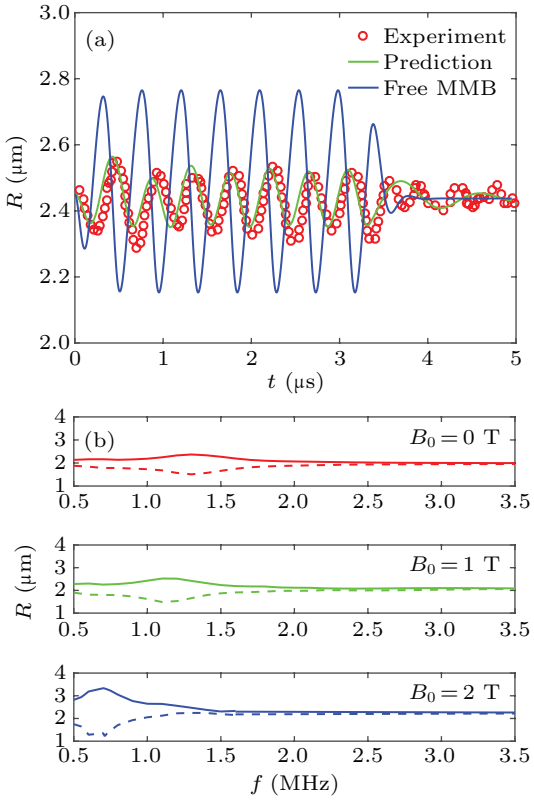


Fig. 8. Pulsation of MMBs near the vessel wall. (a) Compared with Garbin's experimental data;[48] (b) oscillating amplitude in various magnetic fields, R_{max} (solid line) and R_{min} (dashed line).

3.3. Coupled motion

The coupled motion of MMBs near the vessel wall is shown in Fig. 9(a). The three cases have similar trends. There is a much stronger response in the case of both fields than in the other cases, which could be ascribed to the synergistic manipulation. On the other hand, the pulsation in both fields is consistent with the non-spherical jet behavior near the vessel wall,[27] indicating that the volume vibration is improved, and then non-spherical deformation and jet generation. However, further studies on jet behavior go beyond our spherical hypothesis of MMBs. If the MMBs are far from the vessel wall and $l_d = 20$ μm, Fig. 9(b) displays the translational motion. The motion toward the wall is weaker in the acoustic field than in the magnetic field, which can be described by the Bjerknes force decays with $(l_d)^2$. The difference between the red and blue lines is attributed to the fact that the Levich drag in both fields is twice the Stokes drag in the magnetic field. Therefore, a rapid translation of the red line is observed at the initial stage and then the blue line approaches quickly as the MMBs approach the wall. This indicates that the translation of MMBs away from the vessel wall is mainly controlled by the magnetic force, while near the wall it is the Bjerknes force. Moreover, the combined application of magnetic and ultrasonic fields is shown with a shorter horizontal distance $x(t)$. The capture of MMBs can be improved by the synergistic effect between magnetic force and Bjerknes force.

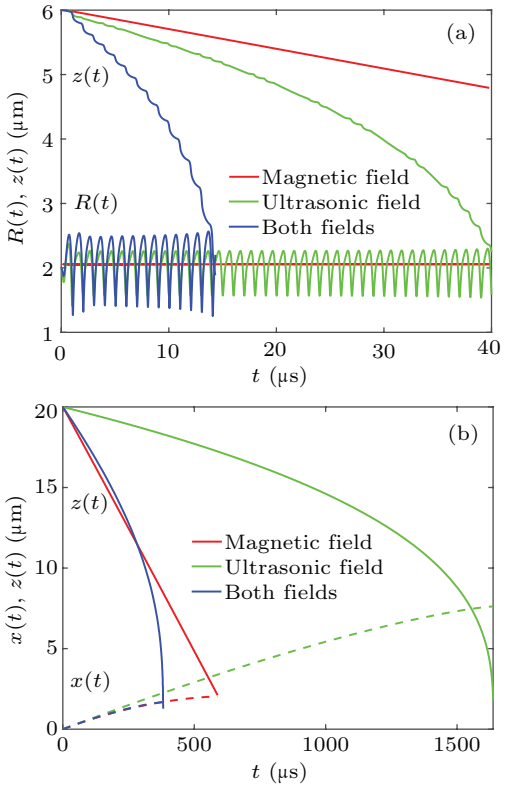


Fig. 9. Coupled motion of MMBs approaching the vessel wall. (a) Close to wall; (b) far from wall.

3.4. Transport distance of drug particles

MMBs carrying drugs and magnetic nanoparticles have the potential to improve localized drug delivery and tumor therapy.[11–13] It is assumed that the slight deformation of the vessel wall is replaced by a rigid wall. In Fig. 10(a), the evolution of transport distance vs. time by solving Eq. (18) and Eq. (23) is compared with the reported trajectory.[12,14] Overall, the similar trend in both results confirms that the model can predict the drug release well. Figures 10(b), 10(c), 10(d) show the influences of B_0, P_a and R_0 on the transport distance, respectively. A stronger magnetic field, higher acoustic pressure and suitable bubble radius provide a further transport distance and allow better drug release. The ultrasound triggers MMBs

with violent vibrations and liquid microstreaming improves the drugs separated from MMBs. For the latter two graphics, the displacement of released drug particles corresponds well with Guillaume's observations,[14] and the existing difference may be explained by the simplified velocity distribution and non-spherical oscillation.

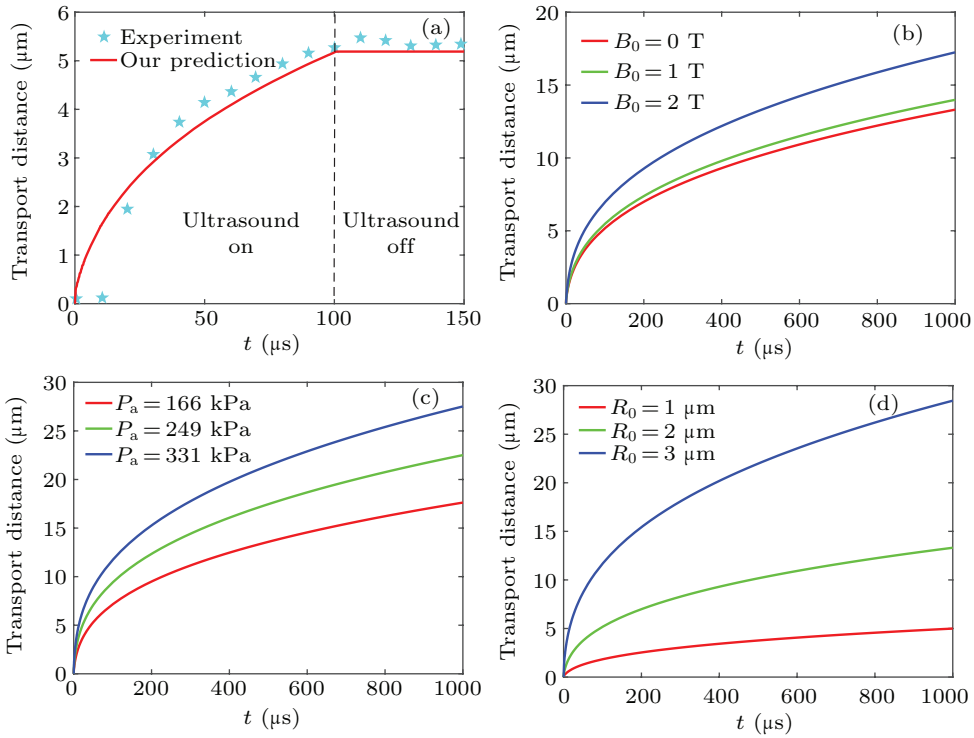


Fig. 10. Transport distance of drug particles. (a) Compared with experimental data in the literature,[25] (b) effects of intensity B_0, (c) effects of driving pressure at $B_0 = 0$ T, (d) effects of MMBs radius at $B_0 = 0$ T.

3.5. Acoustic streaming

Acoustic streaming pattern and direction are usually related to the acoustic driving frequency and amplitude. Streamlines help clarify the trajectory of drug release.[14] Simulated results are shown in Fig. 11(a). Compared to Marmottant's pattern,[51] our

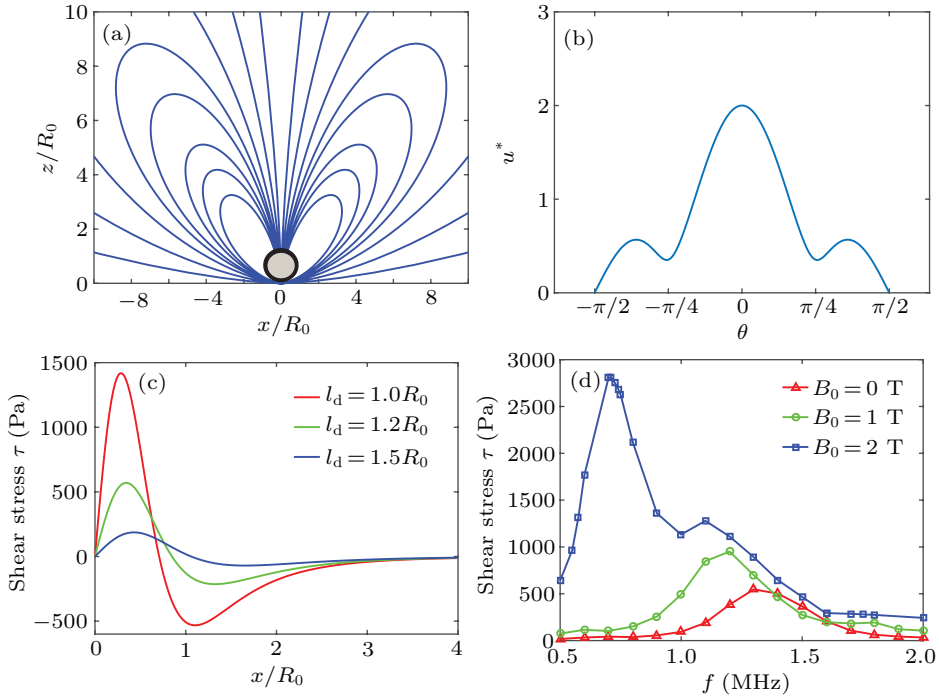


Fig. 11. Mechanical effect associated with vibrating MMBs near the vessel wall. (a) Streamline distribution; (b) spatial dimensionless velocity; (c) shear stress associated with MMB position ($f = 1$ MHz); (d) shear stress determined by acoustic driving frequency f and B_0 at $x/R_0 = 0.4$, $l_d = R_0$.

calculation provides a surprisingly similar streamline distribution away from the bubble center. It is beneficial to understand the process of drug particle release from oscillating MMBs. The non-dimensional release velocity u^* as a function of spatial angle θ is shown in Fig. 11(b). The release velocity u^* is strongly dependent on the streaming direction and distribution; its maximum value is obtained at $\theta = 0$. Figure 11(c) is shear stress distribution on vessel wall when the bubble oscillates at a distance l_d, the negative stress means an opposite direction. At the position of $x/R_0 = 0.3$, the variation in shear stress with driving frequency is shown in Fig. 11(d); the maximum value corresponds to the resonance frequency being driven. This indicates that the combined magnetic and ultrasonic fields could improve shear stress, which may generate sonoporation to enhance transfection,[8,27] and the sonothrombolysis test implies that a better lysis rate is achieved by more cavitation nuclei retained in magnetic targeting region.[11]

3.6. Therapy effect analysis

As noted above, the behavior of MMBs driven by external fields was numerically analyzed, and the results are consistent with the experimental data in the literature. Experiments[8,11,12] reported that the differences in aggregated drug particles in the tumor area caused by external fields eventually lead to different therapeutic effects.[12,13] Lind[27] suggested that a stronger jet formed by the combined application of acoustic–magnetic fields and the generated high-speed collapse is most likely to maximize cell poration and gene/drug delivery. Our observations indicate that the magnitude of shear stress near the vessel wall was increased under applied external fields. In contrast, a uniform magnetic field is verified to weaken the oscillating gas bubble without coated magnetic particles, and is supported by inhibition of sonoluminescence[52–54] and reduction of the blood–brain barrier opening volume.[55] These facts could serve as contrary evidence to approve the model in this work; fiercer pulsation of MMBs is achieved by combined acoustic and magnetic fields. A higher shear stress caused oscillating MMBs in the combined acoustic and magnetic fields, which aligns with the results[11–13] in sonothrombolysis and tumor therapy. The magnetic force makes more MMBs stay in the target area and magnetic pressure improves the pulsation amplitude. The higher shear stress on the vessel wall is expected to enhance drug delivery efficiency.

4. Conclusions

An analytical model of single MMBs, which are transported in blood vessel and exposed to ultrasound and magnetic fields, was established. Our simulation includes translation, vibration and coupled motion of both. Vibration streaming, shear stress and their effects related to particle capture are also predicted. The results suggest that both transport and pulsation are well manipulated by the magnetic field due to the magnetic force and magnetic pressure. The effects of the vessel wall and external fields on the resonance frequency are further evaluated. Acoustic streaming near the vessel wall is demonstrated; some parameters related to drug release are quantified and consistent with the experimental data in the literature. In summary, a combined application of ultrasound and magnetic fields not only improves the capture of MMBs in the targeted region but also increases the shear stress near the vessel wall, which may enhance the permeability of the tissue, thus leading to better drug uptake. These results provide better understanding of the mechanism of MMBs in clinical applications and can be used to optimize the delivery strategy.

Acknowledgement

Project supported by the National Natural Science Foundation of China (Grant Nos. 12074238, 11974232, and 11727813).

References

[1] Owen J, Crake C, Lee J Y, Carugo D, Beguin E, Khrapitchev A A, Browning J R, Sibson N and Stride E 2018 *Drug Deliv. Transl. Res.* **2** 342
[2] Zhang B, Kim H, Wu H, Gao Y and Jiang X 2019 *Ultrasonics* **98** 62
[3] Yang F, Gu Z, Jin X, Wang H and Gu N 2013 *Chin. Phys. B* **22** 104301
[4] Poehlmann M, Grishenkov D, Kothapalli S V, Härmark J, Hebert H, Philipp A, Hoeller R, Seuss M, Kuttner C and Margheritelli S 2014 *Soft Matter* **10** 214
[5] Guo H, Jiang Z, Song S, Dai T, Wang X, Sun K, Zhou G and Dou H 2016 *J. Colloid Interface Sci.* **482** 95
[6] Niu C, Wang Z, Lu G, Krupka T M, Sun Y, You Y, Song W, Ran H, Li P and Zheng Y 2013 *Biomaterials* **34** 2307
[7] Duan L, Yang F, Song L, Fang K, Tian J, Liang Y, Li M, Xu N, Chen Z, Zhang Y and Gu N 2015 *Soft Matter* **11** 5492
[8] Stride E, Porter C, Prieto A G and Pankhurst Q 2009 *Ultrasound Med. Biol.* **35** 861
[9] Mulvana H, Eckersley R J, Browning R, Hajnal J V, Stride E, Barrack T, Tang M, Pankhurst Q and Wells D 2010 *Proc. IEEE Int. Ultrason. Symp.*
[10] Vlaskou D, Mykhaylyk O, Krotz F, Hellwig N, Renner R, Schillinger U, Gleich B, Heidsieck A, Georg Schmitz G, Hensel K and Plank C 2010 *Adv. Funct. Mater.* **20** 3881
[11] de Saint Victor M, Barnsley L C, Carugo D, Owen J, Coussios C C and Stride E 2018 *Ultrasound Med. Biol.* **45** 1151
[12] Gao Y, Chan C U, Gu Q, Lin X, Zhang W, Yeo D C L, Alsema A M, Arora M, Chong M S K, Shi P, Ohl C D and Xu C 2016 *NPG Asia Mater.* **8** e260
[13] Beguin E, Gray M D, Logan K A, Nesbitt H, Sheng Y, Kamila S, Barnsley L C, Bau L, McHale A P, Callan J F and Stride E 2020 *J. Control. Release* **317** 23
[14] Lajoinie G, Luan Y, Gelderblom E, Dollet B, Mastik F, Dewitte H, Lentacker I, de Jong N and Versluis M 2018 *Comm. Phys.* **1** 1
[15] Fang Y, Zhang M, He W, Chen P, Cai X, Yang L, Gu N and Wu J 2011 *Small* **7** 902
[16] Mulvana H, Eckersley R, Tang M X, Pankhurst Q and Stride E 2012 *Ultrasound Med. Biol.* **38** 864
[17] Guo G, Lu L, Yin L, Tu J, Guo X, Wu J, Xu D and Zhang D 2014 *Phys. Med. Biol.* **59** 6729
[18] Gu Y, Chen C, Tu J, Guo X, Wu H and Zhang D 2016 *Ultrason. Sonochem.* **29** 309
[19] Zhao X, Quinto-Su P A and Ohl C D 2009 *Phys. Rev. Lett.* **102** 024501
[20] Roovers S, Lajoinie G, De Cock I, Brans T, Dewitte H, Braeckmans K, Versluis M, De Smedt S and Lentacker I 2019 *Biomaterials* **217** 119250

[21] Yang Y, Li Q, Guo X, Tu J and Zhang D 2020 *Ultrason. Sonochem.* **67** 105096

[22] Sheng Y, Beguin E, Nesbitt H, Kamila S, Owen J, Barnsley L C, Callan B, O'Kane C, Nomikou N, Hamoudi R, Taylor M A, Love M, Kelly P, O'Rourke D, Stride E, McHale A P and Callan J F 2017 *J. Control. Release* **262** 192

[23] Roovers S, Deprez J, Priwitaningrum D, Lajoinie G, Rivron N, Declercq H, De Wever O, Stride E, Le Gac S, Versluis M, Prakash J, De Smedt S C and Lentacker I 2019 *J. Control. Release* **316** 79

[24] Barnsley L C, Carugo D, Aron M and Stride E 2017 *Phys. Med. Biol.* **62** 2333

[25] Barnsley L C, Gray M D, Beguin E, Carugo D and Stride E 2018 *Adv. Mater. Technol.* **3** 1800081

[26] Zhao L, Shi H, Bello I, Hu J, Wang C and Mo R 2022 *Chin. Phys. B* **31** 034302

[27] Lind S J 2014 *Phys. Fluids* **26** 061901

[28] Malvar S, Gontijo R G and Cunha F R 2018 *J. Eng. Math.* **108** 143

[29] Chen J, Zhao L, Wang C and Mo R 2021 *J. Magn. Magn. Mater.* **538** 168293

[30] Doinikov A A, Haac J F and Dayton P A 2009 *Ultrasonics* **49** 269

[31] Zudin Y B, Isakov N S and Zenin V V 2014 *J. Eng. Phys. Thermophys.* **87** 1

[32] Tomita Y, Robinson P B, Tong R P and Blake J R 2002 *J. Fluid Mech.* **466** 259

[33] Doinikov A A 2002 *Phys. Fluids* **14** 1420

[34] Kinefuchi K and Kobayashi H 2018 *Phys. Fluids* **30** 062101

[35] Magnaudet J and Legendre D 1998 *Phys. Fluids* **10** 550

[36] Vlachomitrou M and Pelekasis N 2021 *Phys. Rev. Fluids* **6** 013601

[37] Sassaroli E and Hynynen K 2005 *Phys. Med. Biol.* **50** 5293

[38] SotoÁ M, Peñas P, Lajoinie G, Lohse D and van der Meer D 2020 *Phys. Rev. Fluids* **5** 063605

[39] Wang L, Tu J, Guo X, Xu D and Zhang D 2014 *Chin. Phys. B* **23** 124302

[40] Nyborg W L 1958 *J. Acoust. Soc. Am.* **30** 329

[41] Segers T and Versluis M 2014 *Lab Chip* **14** 1705

[42] Dzaharudin F, Ali N M, Alias E A and Jamaludin U K 2018 *MATEC Web of Conferences* **225** 04015

[43] Deng J, Yang R and Lu H 2021 *Ultrason. Sonochem.* **71** 105371

[44] Beekers I, Van Rooij T, Van d S A F W, de Jong N, Verweij M D and Kooiman K 2019 *IEEE Trans. Ultrason. Ferroelect. Freq. Contr.* **66** 244

[45] Van der Meer S M, Dollet B, Voormolen M M, Chin C T, Bouakaz A, de Jong N, Versluis M and Lohse D 2007 *J. Acoust. Soc. Am.* **121** 648

[46] Sassaroli E and Hynynen K 2005 *Phys. Med. Biol.* **50** 5293

[47] Oguz H N and ProsperettiA 1998 *J. Acoust. Soc. Am.* **103** 3301

[48] Garbin V, Cojoc D, Ferrari E, Di Fabrizio E, Overvelde M L J, van der Meer S M, de Jong N, Lohse D and Versluis M 2007 *Appl. Phys. Lett.* **90** 114103

[49] Hosseinkhah N and Hynynen K 2012 *Phys. Med. Biol.* **57** 785

[50] Mifsud J, Lockerby D A, Chung Y M and Jones G 2021 *Phys. Fluids* **33** 122114

[51] Marmottant P and Hilgenfeldt S 2003 *Nature* **423** 153

[52] Young J B, Schmiedel T and Kang W 1996 *Phys. Rev. Lett.* **77** 4816

[53] Yasui K 1999 *Phys. Rev. E* **60** 1759

[54] Behnia S, Mobadersani F, Yahyavi M, Rezavand A, Hoesinpour N and Ezzat A 2015 *Chaos Solitons Fractals* **78** 194

[55] Yang Y, Pacia C P, Ye D, Yue Y, Chien C Y and Chen H 2021 *Radiology* **300** 681